Convective heat transport in stratified atmospheres at low and high Mach number

Evan H. Anders and Benjamin P. Brown
Department of Astrophysical & Planetary Sciences, University of Colorado – Boulder and Laboratory for Atmospheric and Space Physics, Boulder, CO

Here we study stratified convection in the context of plane-parallel polytropically stratified atmospheres. We hold the density stratification (n_ρ) and Prandtl number (Pr) constant while varying the Mach number (Ma) and the Rayleigh number (Ra) to determine the behavior of the Nusselt number (Nu), which quantifies the efficiency of convective heat transport. As Ra increases and Ma $\to 1$, a scaling of Nu $\propto$ Ra$^{0.45}$ is observed. As Ra increases to a regime where Ma ≥ 1, this scaling gives way to a weaker Nu $\propto$ Ra$^{0.20}$. In the regime of Ma $\ll 1$, a consistent Nu $\propto$ Ra$^{0.3}$ is retrieved, reminiscent of the Nu $\propto$ Ra$^{2/7}$ seen in Rayleigh-Bénard convection.

INTRODUCTION

Convection is essential to heat transport in the cores of high mass stars, the envelopes of low mass stars, and the atmospheres of terrestrial and jovian planets. In such systems, convection occurs in the presence of the atmospheric stratification which can be small but extends up to 14 density scale heights in the Sun's convective envelope. A basic understanding of the properties of compressible convection in stratified media is important to understanding systems in astrophysics and planetary sciences. Numerical constraints have often restricted studies of stratified convection to moderately high Mach numbers, appropriate to regions near the Sun's surface. As such, we know few fundamental properties of the low-Mach number stratified convection which occurs in the deep solar interior.

Early numerical experiments on stratified convection in two [1–4] and three [5, 6] dimensions revealed a number of basic properties in the moderate-to-high Mach number regime. In the widely-studied Rayleigh-Bénard (hereafter RB) problem, upflows and downflows are symmetrical and the temperature gradient approaches zero in the convective interior causing the conductive flux to similarly disappear. Highly stratified convection exhibits narrow downflow lanes and broad upflow regions. Furthermore, the *entropy* gradient is negated by convection rather than the temperature gradient, such that in the presence of perfectly efficient convection a significant component of the flux is still carried by conduction.

In RB convection, there exist two primary control parameters: the Rayleigh number (Ra), the ratio of buoyant driving to diffusive damping, and the Prandtl number (Pr), the ratio of viscous to thermal diffusivity. These numbers couple with the aspect ratio of the physical domain and the boundary conditions to entirely control the dynamics of the convection. In stratified atmospheres, in addition to specifying the equation of state and fundamental properties of the gas, the two control parameters of RB convection are joined by the degree of stratification across the domain and the characteristic Mach number (Ma) of the convective flows. Polytropically stratified atmospheres, such as those used in early studies, are an ideal extension of RB convection into the stratified realm as the two additional control parameters are directly linked to basic properties of the atmosphere. The density stratification is set by the number of density scale heights the atmosphere spans (n_ρ), and Ma is controlled by the superadiabatic excess (ϵ), the deviation of the polytropic index from the adiabatic polytropic index [1].

In this letter we study the behavior of convective heat transport, quantified by the Nusselt number (Nu), in plane-parallel two-dimensional polytropically stratified atmospheres. We vary ϵ and Ra while holding $n_\rho$and Pr constant across all simulations. We study domains with an aspect ratio of 4. In section II, we describe the construction of atmospheres, our equations, and our method for numerical time evolution. We describe our findings in section III and discuss implications in section IV.

EXPERIMENT

In order to compare our results with previous studies and in an effort to examine a simplest case, we study a fluid composed of monatomic ideal gas particles with an adiabatic index of $\gamma = 5/3$ and whose equation of state is $P = R\rho T$. The initial stratification is polytropic and the gravitational acceleration and conductive heat flux are invariant throughout the depth of the atmosphere. We specify that both the thermal conductivity, κ, and the temperature gradient, ∇T_0, are constant while constructing our atmosphere such that $\boldsymbol{F}_{\mathrm{cond},0} = -\kappa\nabla T_0 = \text{constant}$. Under these assumptions, solving the equation of hydrostatic equilibrium produces an atmosphere defined by

$$\begin{aligned} \rho_0(z) &= \rho_{00}(z_0 - z)^m \\ T_0(z) &= T_{00}(z_0 - z). \end{aligned} \tag{1}$$

Thermodynamic variables are nondimensionalized at the top of the atmosphere as $P_0(L_z) = \rho_0(L_z) = T_0(L_z) = 1$, requiring $z_0 \equiv L_z + 1$ and $R = T_{00} = \rho_{00} = 1$. By this choice, the non-dimensional length scale is the inverse temperature gradient scale and the timescale is the

isothermal sound crossing time of this unit length. z increases upwards within the bounds $z = [0, L_z]$, where $L_z = e^{n_\rho/m} - 1$ is determined by the number of density scale heights the atmosphere spans, n_ρ. Throughout this letter, we set $n_\rho = 3$ such that the density varies by a factor of 20. The polytropic index is such that $m = m_{ad} - \epsilon$ where $m_{ad} \equiv (\gamma - 1)^{-1}$ is the adiabatic polytropic index and ϵ is the superadiabatic excess. The subsequent entropy gradient at the top of the atmosphere is $\nabla S(L_z) = -\epsilon$. The characteristic timescale of convective dynamics is related to the atmospheric buoyancy time, $t_{\rm b} = \sqrt{L_z/g\epsilon}$, with $g = (m + 1)$. We will utilize buoyancy time units throughout this letter.

Atmospheric diffusivities are specified by the Rayleigh number and the Prandtl number. The non-dimensional Rayleigh number is

$$\mathrm{Ra} = \frac{g L_z^3 (\Delta S_0 / c_P)}{\nu \chi}, \tag{2}$$

where ΔS_0 is the entropy difference between the top and bottom of the atmosphere, $c_P = R\gamma(\gamma - 1)^{-1}$ is the specific heat at constant pressure, ν is the kinematic viscosity (viscous diffusivity), and χ is the thermal diffusivity. The relationship between the thermal and viscous diffusivities is set by the Prandtl number, Pr$= \nu/\chi$. We relate the dynamic viscosity, μ, and the thermal conductivity, κ, to their corresponding diffusivities such that $\nu \equiv \mu/\rho$ and $\chi \equiv \kappa/\rho$. As a result, Ra $\propto (\nu\chi)^{-1} \propto \rho^2$. The atmospheres studied here with $n_\rho = 3$ experience an increase in the Rayleigh number by a factor of 400 across the domain. This formulation leaves Pr constant throughout the depth of the atmosphere, and in this letter we impose Pr = 1. Throughout this letter, we specify Ra at the top of the atmosphere.

At the constant values of n_ρ and Pr used, the primary control parameters of convection are ϵ and Ra. We decompose our atmosphere into the background polytrope $(\ln \rho_0, T_0)$ and the fluctuations about that background $(\boldsymbol{u}, \ln \rho_1, T_1)$. The scaling of the entropy gradient with ϵ is reflected in the evolved values of these fluctuations, which follow the scaling of $T_1/T_0 \propto \rho_1/\rho_0 \propto \mathrm{Ma}^2 \propto \epsilon$ for low values of ϵ, as in Fig. 1.

We evolve the Fully Compressible Navier-Stokes equations, which take the form:

$$\frac{D \ln \rho}{Dt} = -\nabla \cdot (\boldsymbol{u}) \tag{3}$$

$$\begin{aligned}\frac{D\boldsymbol{u}}{Dt} =& -\nabla T - T\nabla \ln \rho + \boldsymbol{g} \\ &+ \nu \nabla \cdot (\bar{\bar{\boldsymbol{\sigma}}}) + \bar{\bar{\boldsymbol{\sigma}}} \cdot \nabla \nu + \nu \bar{\bar{\boldsymbol{\sigma}}} \cdot \nabla \ln \rho\end{aligned} \tag{4}$$

$$\begin{aligned}\frac{DT}{Dt} =& -(\gamma - 1) T \nabla \cdot (\boldsymbol{u}) + \frac{1}{c_V} \left(\chi \nabla^2 T + \nabla T \cdot \nabla \chi \right. \\ &\left. + \chi \nabla T \cdot \nabla \ln \rho + \nu \left[\bar{\bar{\boldsymbol{\sigma}}} \cdot \nabla \right] \cdot \boldsymbol{u} \right)\end{aligned} \tag{5}$$

where $D/Dt \equiv \partial_t + \boldsymbol{u} \cdot \nabla$ and the viscous stress tensor is

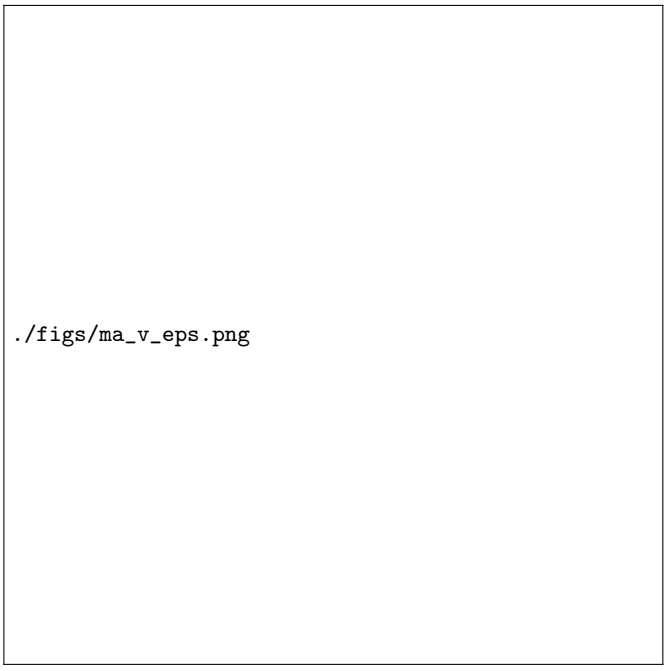

FIG. 1. (a) Characteristic horizontally averaged maximum Mach numbers have been time averaged for over $\geq 100 t_b$ beginning roughly $50 t_b$ after the start of simulations. For $\epsilon \leq 0.1$, an evident scaling of $Ma \propto \{\epsilon^{0.50}, \epsilon^{0.51}\}$ at Ra $= \{10^2, 10^5\}$ is retrieved. When $\epsilon \to m_{ad}$, large deviations from this power law are seen and the systems display supersonic dynamics. (b) At high epsilon, Ma scales as $\mathrm{Ra}^{0.28}$ until it reaches the supersonic regime, at which point it turns over and follows a power law of $\mathrm{Ra}^{-0.10}$. At low epsilon, consistent power laws are achieved throughout all values of *Ra* studied, where Ma $\propto \{\mathrm{Ra}^{0.26}, \mathrm{Ra}^{0.22}\}$ for $\epsilon = \{10^{-4}, 10^{-7}\}$. All error bars are negligible.

defined as

$$\sigma_{ij} \equiv \left(\frac{\partial u_i}{\partial x_j} + \frac{\partial u_j}{\partial x_i} - \frac{2}{3} \delta_{ij} \nabla \cdot (\boldsymbol{u}) \right). \tag{6}$$

In such stratified systems, the total convective flux is

$$\boldsymbol{F}_{\rm conv} \equiv \boldsymbol{F}_{\rm enth} + \boldsymbol{F}_{\rm KE} + \boldsymbol{F}_{\rm PE} + \boldsymbol{F}_{\rm visc}, \tag{7}$$

where $\boldsymbol{F}_{\rm enth} \equiv \rho \boldsymbol{u}(c_V T + P/\rho)$ is the enthalpy flux, $\boldsymbol{F}_{\rm KE} \equiv \rho |\boldsymbol{u}|^2 \boldsymbol{u}/2$ is the kinetic energy flux, $\boldsymbol{F}_{\rm PE} \equiv \rho \boldsymbol{u} \phi$ is the potential energy flux (with $\phi \equiv -gz$), and $\boldsymbol{F}_{\rm visc} \equiv -\rho\nu\boldsymbol{u} \cdot \bar{\bar{\boldsymbol{\sigma}}}$ is the viscous flux. Taking an inner product of Eq. 4 with $\boldsymbol{u}$ and adding it to Eq. 5, the full energy equation in conservation form is retrieved,

$$\frac{\partial}{\partial t} \left(\rho \left[\frac{|\boldsymbol{u}|^2}{2} + c_V T + \phi \right] \right) + \nabla \cdot (\boldsymbol{F}_{\rm conv} + \boldsymbol{F}_{\rm cond}) = 0 \tag{8}$$

where $\boldsymbol{F}_{\rm cond} = -\kappa \nabla T$. An understanding of the flux terms is essential to characterizing the convective heat transport in our systems.

The atmosphere is contained between two impenetrable, stress free, fixed temperature boundaries at the top

and bottom of the domain such that $w = \partial_z u = T_1 = 0$ at $z = \{0, L_z\}$. The domain is periodic in the horizontal. We utilize the novel Dedalus[1] pseudospectral framework to time-evolve Eqs. 3-5 using an implicit-explicit third-order four-step Runge-Kutta timestepping scheme RK443 [7]. Variables are time-evolved on a dealiased Chebyshev (vertical) and Fourier (horizontal) domain in which the physical grid dimensions are 3/2 the size of the coefficient grid. Our physical grid sizes range from 96x384 grid points at the lowest values of Ra to 1152x4608 grid points at Ra $\geq 10^7$. By using IMEX timestepping, we implicitly step the stiff linear acoustic wave contribution and we are able to efficiently study flows at moderate ($Ma \approx 1$) and very low ($Ma \approx 10^{-4}$) Mach number (Fig. 1b). Our equations take the form of the FC equations in [8], extended to include variable ν and χ, and we follow the approach there; this IMEX approach has been successfully tested against a nonlinear benchmark of the compressible Kelvin-Helmholtz instability [9].

RESULTS

The efficiency of convection is quantified by the Nusselt number. While the Nusselt number is well-defined in RB convection as the amount of total flux divided by the steady-state background conductive flux [10, 11], a well-defined Nusselt number is more elusive in stratified convection. A traditional definition of the Nusselt number in stratified convection is [1, 3]

$$\mathrm{Nu} \equiv \frac{F_{\mathrm{conv,\,z}} + F_{\mathrm{cond,\,z}} - F_A}{F_{\mathrm{ref}} - F_A}, \tag{9}$$

where $F_{\mathrm{conv,\,z}}$ and $F_{\mathrm{cond,\,z}}$ are the z-components of $\boldsymbol{F}_{\mathrm{conv}}$ and $\boldsymbol{F}_{\mathrm{cond}}$, respectively. F_A is the adiabatic conductive flux, defined as $F_A = -\kappa \partial_z T_{\mathrm{ad}}$. For an ideal gas in hydrostatic equilibrium, $\partial_z T_{\mathrm{ad}} \equiv -g/c_P$. $F_{\mathrm{ref}} = \Delta T / L_z$, where $\Delta T = T(L_z) - T(0)$, is the conductive flux of a linear profile connecting the upper and lower plates, which is constant for the choice of fixed-temperature boundaries.

We contend that this is the general form of the Nusselt number. To illustrate this, we consider a few limiting cases. Convection works to suppress entropy stratification and create isentropic atmospheres. Under the Boussinesq approximation, density variations are ignored and entropy stratification is directly proportional to temperature stratification, such that $\nabla S \to 0$ only when $\nabla T \to 0$. Thus, for RB convection, $\nabla T_{\mathrm{ad}} \equiv 0$ and the familiar form of Nu is retrieved. In the case of stratified convection, as $\epsilon \to m_{ad} + 1$, $\nabla P \propto g \to 0$ and the resulting $\nabla T_{\mathrm{ad}} \to 0$. In such a case, $F_A \to 0$ and the definition of the RB Nu is appropriate to use, as convection carries all of the flux [12]. As $\epsilon \to 0$, $\nabla T_{\mathrm{ad}} \to \nabla T_0$, the atmospheric initial temperature profile. This causes increasingly smaller velocity, and thermodynamic perturbations (e.g. Fig. 1), but the removal of the O(1) background term in the numerator and denominator of Eq. 9, makes the numerator and denominator both O(ϵ).

We solved initial value problems which start in hydrostatic and thermal equilibrium and experienced infinitesimal kicks compared to ϵ in T_1. Solutions were time-evolved until a long-time average of Nu showed little dependence on depth. By performing a linear stability analysis, we determined that the onset of convection occurs at $\mathrm{Ra}_c = \{10.06, 10.97, 10.97\}$ for $\epsilon = \{0.5, 10^{-4}, 10^{-7}\}$, respectively. We study Rayleigh numbers from values at onset up to nearly $10^6\mathrm{Ra}_c$ for $\epsilon = 0.5$, $10^5\mathrm{Ra}_c$ for $\epsilon = 10^{-4}$, and $10^4\mathrm{Ra}_c$ for $\epsilon = 10^{-7}$. At high values of ϵ, shock systems form in the upper atmosphere near downflow lanes (Fig. 2a) and propagate towards upflow lanes. These shocks heat downflowing material which reduces the efficiency of convective transport. Such systems were reported in both two [4] and three [13] dimensional poly-

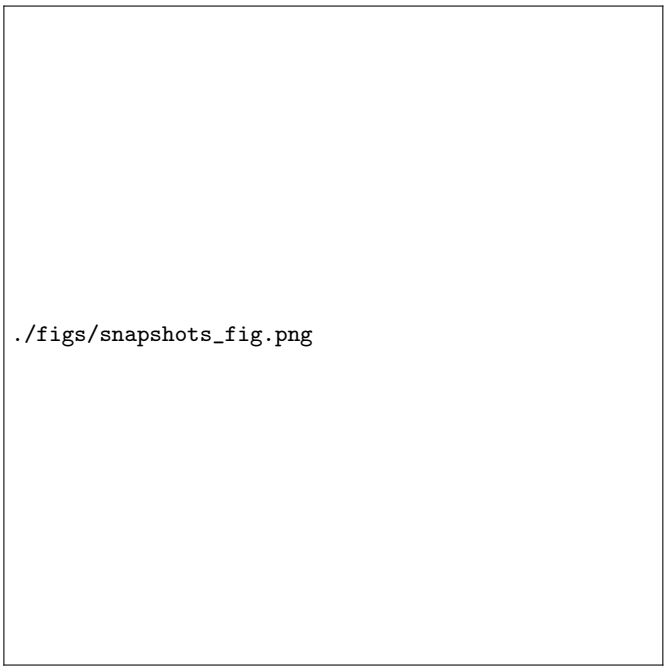

FIG. 2. Characteristic entropy fluctuations in evolved flows. The time- and horizontally- averaged profile is removed in all cases. At high ϵ (a), shock systems form near the upper downflow lanes and propel shock-heated material deep within the atmosphere at sufficiently high Ra. At low ϵ but at the same Ra (b), shock systems are absent, but otherwise the dynamics are similar. As Ra is increased (c), downflow lanes no longer span the entirety of the domain and individual small blobs are responsible for carrying the flux.

[1] http://dedalus-project.org/

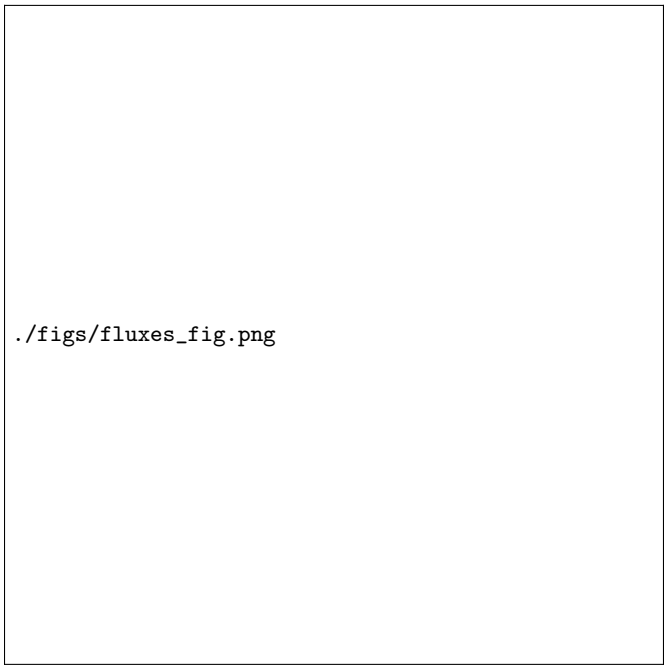

FIG. 3. Time-averaged flux profiles for high (top) and low (bottom) Mach number flows at $Ra = 10^6$. The dashed lines correspond to the enthalpy flux (orange, positive) and kinetic energy flux (purple, negative). The grey dash-dot line is the viscous flux, the blue dash-dot-dot line is the potential energy flux, and the green dotted line is the radiative flux with the adiabatic radiative flux removed. All fluxes are normalized by $F_{ref} - F_A$, as in the calculation of the Nusselt number. The solid black line is the properly normalized sum of all the fluxes, and under this normalization its height-averaged value is the Nusselt number.

tropic simulations previously. These shocks heat material entering the downflows, reducing both the buoyant driving and the efficiency of convective transport there.

Low mach number flows, such as those in an $\epsilon = 10^{-4}$ atmosphere (Fig. 2b) have similar bulk thermodynamic structure but lack the complicating dynamics of shock heating. This is interesting in light of the current literature, as low Mach number flows are in pressure equilibrium with the background and pressure forces cannot be the cause of narrow downflow lanes and broad upflow regions, as has been suggested [3]. As Ra is increased to very large values (Fig. 2c), thermodynamic structures break up into small packets which traverse through the domain many times before diffusing rather than spanning the whole domain. The complicated nature of high Ra dynamics, especially in the low Ma regime where shocks are absent, has barred us from sufficiently converging any solutions in the regime of Ra $> 10^5 \mathrm{Ra}_c$ at low ϵ.

At high values of Ra, the heat transport properties of the systems become increasingly complex and time-dependent. Large ϵ flows exhibit two local maxima in the enthalpy flux and kinetic energy flux: one in the upper atmosphere caused by the shocks, and one in the lower atmosphere caused by the deep mixing of convective motions (see Fig. 3a). At low ϵ, only the deep maximum is present (Fig. 3b). Furthermore, the presence of fixed-temperature boundary conditions allows the flux at the boundaries to vary. Many runs at $Ra > 10^5$ and $\epsilon = 10^{-4}$ exhibit time-dependent states of stratified convection (such as those shown in Fig. 2b&c), in which the flux entering the system at the bottom of the atmosphere exceeds that at the top. These states are punctuated by states of vigorous shearing, similar to those previously reported in two-dimensional RB convection [14]. These shearing states flatten the bottom temperature gradient towards adiabatic, allowing the excess energy to exit through the upper boundary. These shearing states will be covered in more detail in a future paper. Regardless, a proper long-term average over shearing and non-shearing states retrieves an invariant flux profile (and therefore Nu profile) throughout the depth of the atmosphere.

After appropriately time-averaging the fluxes, a sensible Nusselt number is retrieved. Nusselt numbers for all simulations at low and high Ma are plotted in Fig. 4. At $\epsilon = \{10^{-4}, 10^{-7}\}$, scaling laws of $Nu \propto Nu^{\{0.31,0.31\}}$ are retrieved. At $\epsilon = 0.5$, in the near-sonic regime ($Ra \leq 10^4$), the scaling of Nu with Ra is inflated, with $Nu \propto Ra^{0.45}$. As simulations pass into the supersonic regime and shocks start to form near the downflows, propelling warm fluid deep into the atmosphere, that scaling drops to $Nu \propto Ra^{0.19}$. Error on all power law scalings is negligible.

DISCUSSION

In this letter we have studied fundamental heat transport by stratified convection in simplified 2-D polytropic atmospheres at low and high Mach number. Our atmospheres here are specified by two parameters, $n_\rho$and ϵ. We argue that these atmospheres are the natural extension of the RB problem to stratified systems, and should be used to understand the basic properties of stratified convection. The similarity between the scaling of Nu in RB convection and in these stratified polytropes suggests that a boundary layer theory such as the Prandtl-Blausius or Grossmann-Lohse theories for incompressible flows could be developed for fully compressible convection in these systems [15].

Furthermore, we have demonstrated that low Ma flows exhibit the same pattern of broad upflows and narrow downflows observed in high Ma flows [3]. At low Ma, flows are often in pressure equilibrium with their surroundings, so cooling parcels increases their density, and both of these effects reduce entropy. Neither of the two free thermodynamic variables can cause breaking in warm upflow regions, so stratification effects must cause the observed flow asymmetry. While not studied in this work, it is possible that at low Ma, flows feel the pres-

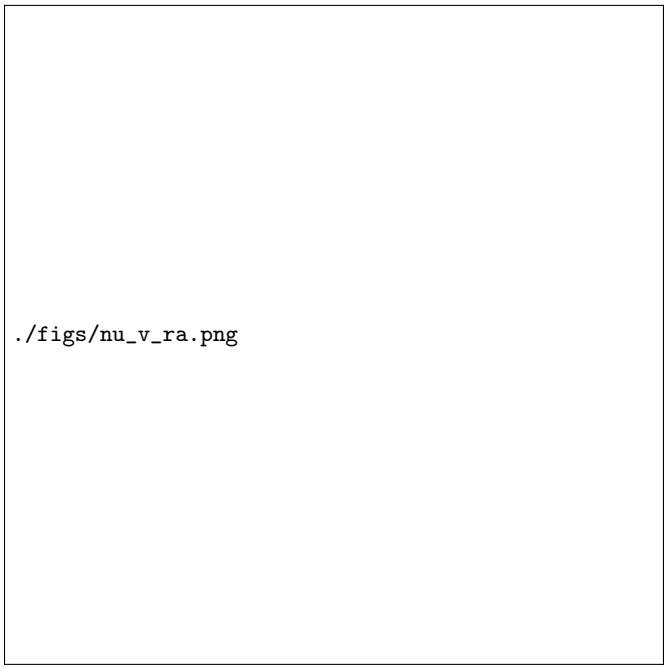

FIG. 4. Variation of Nu as Ra increases is shown for $\epsilon = \{10^{-7}, 10^{-4}, 0.5\}$. At high ϵ, a clear transition from the subsonic to supersonic regime is evident in the scaling of Nu with Ra. In the low ϵ regime Nu vs. Ra scalings collapse onto a similar line which is reminiscent of RB scalings [10]. Error bars represent one standard deviation of a long-time averaged Nu sampled throughout the depth of the domain.

sure response of the boundaries, causing deflection in a manner unseen at high Ma.

The dynamics of these polytropic solutions are complex and highly time-dependent, even in two dimensions. Time-dependent oscillating shear states have developed spontaneously, as seen before in RB convection [14]. While computationally difficult, the highest values of Ra and the lowest value of ϵ studied here are far below the values found in nature. If the scalings of Nu and Ma presented here hold, then under solar conditions (Ra $\approx 10^{20}$, Ma $\approx 10^{-4}$), we expect that $\epsilon \approx 10^{-20}$ and Nu $\approx 10^{6}$.

Future work will aim to better understand the mechanisms of shearing states and whether or not these states are attainable in three-dimensional, non-rotating atmospheres. Our studies here have set the groundwork for understanding and comparing heat transport in stratified convection to that in RB convection [10], and for future studies of transport in stratified convection in more realistic systems, such as those bounded by stable regions [**?**] or using more realistic profiles of κ.

acknowledgements

This work was supported by the CU/NSO George Ellery Hale Graduate Fellowship and supported by NASA LWS grant number NNX16AC92G. Computations were conducted with support by the NASA High End Computing (HEC) Program through the NASA Advanced Supercomputing (NAS) Division at Ames Research Center with allocations (GID s1647, PI Brown; GID g26133, PI Toomre). We thank Axel Brandenburg, Mark Rast, and Jeff Oishi for many useful discussions.

[1] E. Graham, Journal of Fluid Mechanics **70**, 689 (1975).
[2] K. L. Chan, S. Sofia, and C. L. Wolff, Astrophys. J. **263**, 935 (1982).
[3] N. E. Hurlburt, J. Toomre, and J. M. Massaguer, Astrophys. J. **282**, 557 (1984).
[4] F. Cattaneo, N. E. Hurlburt, and J. Toomre, ApJL **349**, L63 (1990).
[5] F. Cattaneo, N. H. Brummell, J. Toomre, A. Malagoli, and N. E. Hurlburt, Astrophys. J. **370**, 282 (1991).
[6] N. H. Brummell, N. E. Hurlburt, and J. Toomre, Astrophys. J. **473**, 494 (1996).
[7] U. M. Ascher, S. J. Ruuth, and R. J. Spiteri, Applied Numerical Mathematics **25**, 151 (1997).
[8] D. Lecoanet, B. P. Brown, E. G. Zweibel, K. J. Burns, J. S. Oishi, and G. M. Vasil, Ap. J. **797**, 94 (2014), 1410.5424.
[9] D. Lecoanet, M. McCourt, E. Quataert, K. J. Burns, G. M. Vasil, J. S. Oishi, B. P. Brown, J. M. Stone, and R. M. O'Leary, MNRAS **455**, 4274 (2016), 1509.03630.
[10] H. Johnston and C. R. Doering, Physical Review Letters **102**, 064501 (2009), 0811.0401.
[11] J. Otero, R. W. Wittenberg, R. A. Worthing, and C. R. Doering, Journal of Fluid Mechanics **473**, 191 (2002).
[12] A. Brandenburg, K. L. Chan, Å. Nordlund, and R. F. Stein, Astronomische Nachrichten **326**, 681 (2005), astro-ph/0508404.
[13] A. Malagoli, F. Cattaneo, and N. H. Brummell, ApJL **361**, L33 (1990).
[14] D. Goluskin, H. Johnston, G. R. Flierl, and E. A. Spiegel, Journal of Fluid Mechanics **759**, 360 (2014).
[15] G. Ahlers, S. Grossmann, and D. Lohse, Rev. Mod. Phys. **81**, 503 (2009).